JOURNAL OF SOLID STATE CHEMISTRY 87, 44–54 (1990)

The Type II Superstructural Family in the Bi_2O_3–V_2O_5 System

WUZONG ZHOU

Department of Chemistry, University of Cambridge, Lensfield Road, Cambridge CB2 1EP, United Kingdom

Received December 27, 1989; in revised form March 12, 1990

Following the work on defect fluorite superstructures in the Bi_2O_3–V_2O_5 system, the detailed structures of the type II family in this system have been investigated by high resolution electron microscopy. For compositions from $6Bi_2O_3$–V_2O_5 to $7Bi_2O_3$–$2V_2O_5$, vanadium cations exist in the form of V_4O_{10} tetrahedral clusters within the δ-Bi_2O_3 lattice. These clusters are ordered, but their arrangement is variable so that many triclinic superstructures exist. © 1990 Academic Press, Inc.

Introduction

Defect fluorite-related solid–solutions in the systems of Bi_2O_3–Nb_2O_5 (*1, 2*), Bi_2O_3–Ta_2O_5 (*3*), and Bi_2O_3–V_2O_5 (*4*) have been previously studied by high resolution electron microscopy (HREM) in these laboratories. Although X-ray diffraction patterns from most samples were identical and could only be indexed onto the δ-Bi_2O_3-like (*5*) unit cells, many superstructures were observed. These superstructures were classified into several types according to the different forms of the guest oxide clusters in the δ-Bi_2O_3 host lattice. In the type I solid–solution, the guest cations are separated from one another (so that there is no M–O–M bonding, M = Nb, Ta, or V), ordered in a body-centered $2 \times 2 \times 2$ cubic superlattice in the Bi_2O_3–M_2O_5 (M = Nb or Ta) systems and in a face-centered $3 \times 3 \times 3$ cubic superlattice in the Bi_2O_3–V_2O_5 system. The type II structures in the Bi_2O_3–M_2O_5 (M = Nb or Ta) systems are also cubic. All M cations are six coordinated by oxygen. Each four such octahedra, MO_6, form a tetrahedral cluster, M_4O_{18}, which links with the fluorite-like bismuth oxide network and together can be regarded as pyrochlore-like units. It is more likely that two or more of these tetrahedral units are joined together to form some larger units, M_7O_{30}, etc., lying on all three (111) planes of the fluorite lattice. However, in the system Bi_2O_3–V_2O_5, vanadium cations are coordinated by four oxygens which was confirmed by a laser Raman study (I. E. Wachs, unpublished). The VO_4 units are usually arranged into V_4O_{10} tetrahedral units and the formation of larger units is impossible, since vanadium cations shared by two V_4O_{10} tetrahedral units would require six coordination of oxygen. The V_4O_{10} tetrahedral clusters lie on only one of the (111) planes of the δ-Bi_2O_3 fluorite lattice, differing from other systems where the clusters lie on all three such planes. The separation of these V_4O_{10}-contained (111) planes, designated main (111) plane, and the arrangement of the V_4O_{10} units within them are variable. Consequently, for the compositions from $6Bi_2O_3$–V_2O_5 to $7Bi_2O_3$–

0022-4596/90 $3.00

$2V_2O_5$, the type II structure in this system is actually a large family of many closely related phases. In the previous work (*4*), the structure of the first member of the type II family (the type IIa) was determined by computer image simulations, and unit cell dimensions were given for the other five members.

Generally, structures of solid–solution materials can be described in a term of "multiorder" approximation; i.e., the basic structure of a solid–solution determined by X-ray diffraction method is a "first-order" approximation and the detailed superstructure revealed by HREM studies is a "second-order" approximation to the truth. The detailed structures found in the δ-Bi_2O_3-based–solid solutions not only are of interest in term of structural chemistry but also they effect the physicochemical properties of these materials (*6*). Some of the solid–solution materials in the Bi_2O_3–V_2O_5 system have also been used as catalysts for partial oxidation of methane and good yields of higher hydrocarbons are produced at 700°C (*7*).

In the present work, structural details of six members of the type II family found in the Bi_2O_3–V_2O_5 system are discussed.

Experimental

Experimental details of this work are identical to those described previously (*4*). Three compositions, $6Bi_2O_3$–V_2O_5, $4Bi_2O_3$–V_2O_5, and $7Bi_2O_3$–$2V_2O_5$, have been prepared. All samples were found to be homogeneous by energy dispersive X-ray spectrometry. Initial characterization of the samples was by X-ray powder diffractometry (XPD). Unlike the type I structure and other fluorite-related solid–solution materials, the XPD spectra of the type II structures in the Bi_2O_3–V_2O_5 system reveal a departure from the cubic symmetry (see Fig. 1f in Ref. (*4*)). However, selected area electron diffraction (SAED) patterns indicated that all the type II structures in this system are still derived from the defect fluorite sublattice. The details of each member are discussed below.

Results and Discussion

Type IIa Structure

The structure of type IIa found in the sample of $6Bi_2O_3$–V_2O_5 has been determined (*4*). The unit cell is triclinic with $a = b = 1.17$, $c = 2.39$ nm, $\alpha = \beta = 57.8°$, and $\gamma = 60.0°$. The relationship between the fluorite sublattice and the type IIa superunit cell can be expressed as

$$a_{IIa} = \tfrac{3}{2}a_f + \tfrac{3}{2}c_f$$

$$b_{IIa} = \tfrac{3}{2}b_f + \tfrac{3}{2}c_f$$

$$c_{IIa} = -a_f - b_f + 4c_f.$$

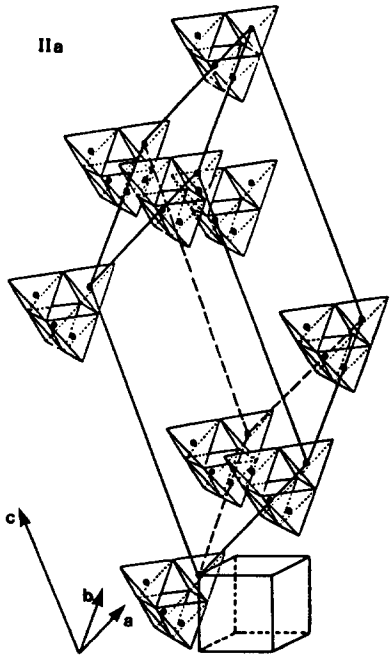

FIG. 1. The V_4O_{10} arrangement in the model for the type IIa superstructure in the system Bi_2O_3–V_2O_5. The cube shows the fluorite subcell (after Zhou (*4*)).

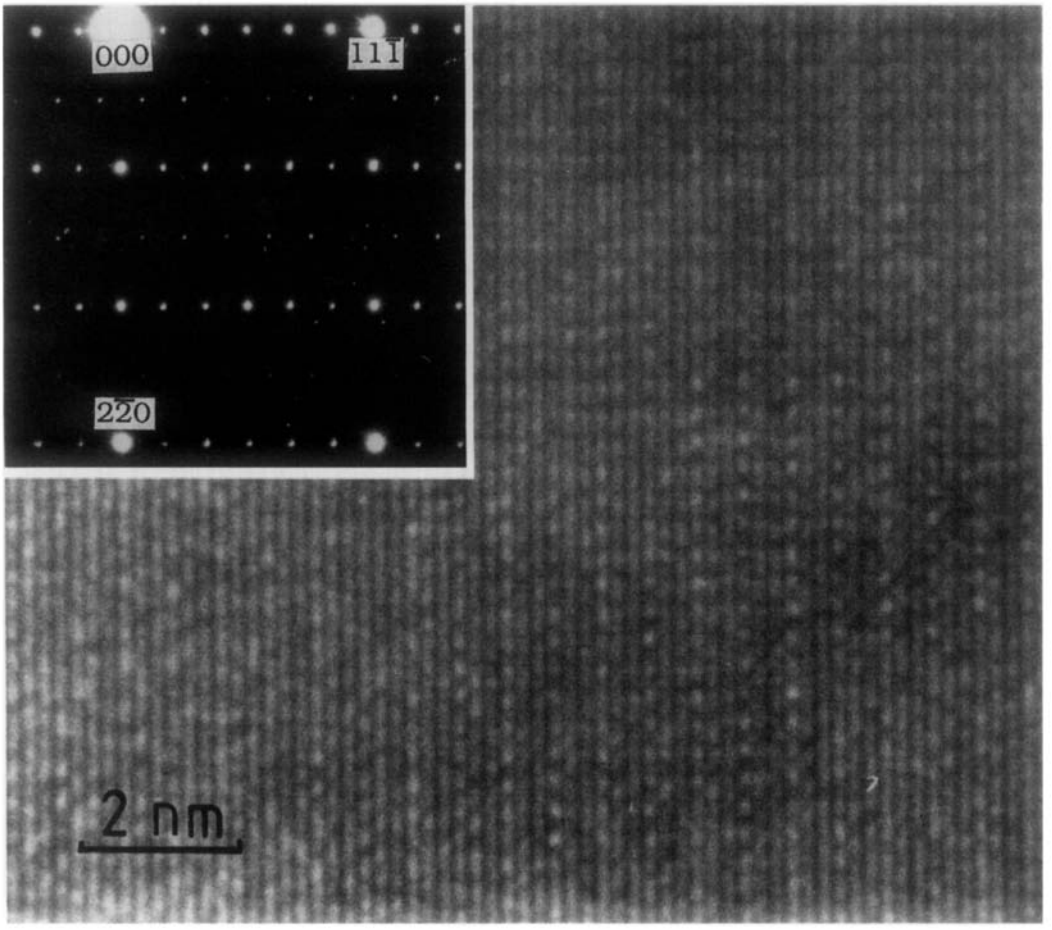

FIG. 2. HREM image and the corresponding SAED pattern of the type IIb structure obtained from $6Bi_2O_3$–V_2O_5, viewed down the [112] direction of the fluorite subcell.

where a, b, c are unit cell vectors. c_{IIa} could also be chosen as $-\frac{5}{2}a_f - \frac{5}{2}b_f + c_f$, etc. The arrangement of V_4O_{10} clusters in type IIa is shown in Fig. 1 as a comparison to the other members.

Since all the superlattices discussed in this work are based on the fluorite-like δ-Bi_2O_3 sublattice with different arrangements of V_4O_{10} clusters inside this sublattice, to emphasize this, only tetrahedral V_4O_{10} clusters are shown in the figures for all models. Therefore, the space between adjacent clusters is filled by bismuth and oxygen atoms. It has to be pointed out that most superstructural models described might have monoclinic symmetries when superunit cell vectors a and b are chosen to be along the $(a_f + b_f + 2c_f)$ and $(a_f - b_f)$ directions, respectively. However, the present work deals mainly with ordered arrangement of V–O guest oxide clusters rather than exact atomic positions and space groups of the superstructures. A triclinic symmetry was chosen for these struc-

tures in order to obtain as small a unit cell as possible and to show the V_4O_{10} arrangement clearly. The real unit cell parameters and space group for each structural member might be determined later by refinement of neutron diffraction if a single phase material can be prepared.

Type IIb Structure

The type IIb structure has a unit cell with the three parameters, a, b, and c, being double those found in the type IIa structure. Figure 2 shows a typical SAED pattern and the corresponding HREM image of the type IIb structure taken from a $6Bi_2O_3$–V_2O_5 sample. HREM images for type IIa and type IIb structures are very similar, suggesting that the type IIb structure is just a slightly modified type IIa.

Although the arrangement of V_4O_{10} tetrahedral clusters within the main (111) plane of the fluorite lattice is almost always the same, there is one vanadium cation in each tetrahedron sitting outside this plane, which can be on either side of the (111) plane. The composition of the (001) plane of the unit cell (i.e., the (111) plane of the fluorite structure) can be thought of as being composed of alternating rows of V_4O_{10} tetrahedra, where one such row (in the $[1\bar{1}0]$ direction in the (001) plane of the unit cell) has the out-of-plane vanadium cations above the (001) unit cell plane, and the adjacent rows have the out-of-plane vanadium cations below the (001) plane. This is illustrated in Fig. 3a. The superunit cell is derived from the fluorite sublattice by the relations

$$a_{\mathrm{IIb}} = 3a_{\mathrm{f}} + 3c_{\mathrm{f}}$$

$$b_{\mathrm{IIb}} = 3b_{\mathrm{f}} + 3c_{\mathrm{f}}$$

$$c_{\mathrm{IIb}} = -2a_{\mathrm{f}} - 2b_{\mathrm{f}} + 8c_{\mathrm{f}},$$

with unit cell parameters $a = b \approx 2.34$ nm, $c \approx 4.79$ nm, $\alpha = \beta \approx 57.8°$, and $\gamma \approx 60.0°$. It is also possible to choose a shorter c_{IIb} as $c_{\mathrm{IIb}} = -5a_{\mathrm{f}} - 5b_{\mathrm{f}} + 2c_{\mathrm{f}}$. The composition of the whole unit cell is $Bi_{368}V_{64}O_{712}$ with 152 oxygen vacancies if all cations keep their original valence. It has been understood that oxygen vacancies tend to associate with the guest cations in the δ-Bi_2O_3-based solid–solutions. The structural type formed is dependent on the oxygen vacancy concentration (*3*).

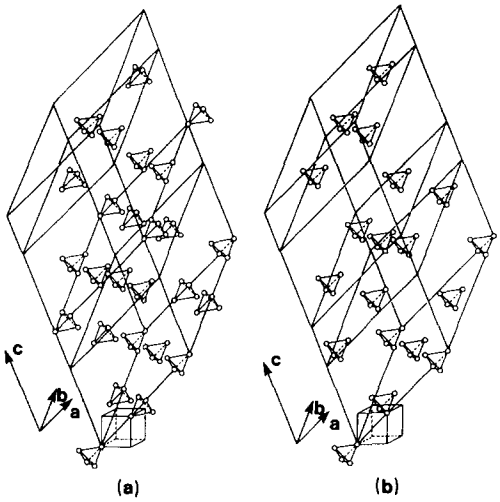

FIG. 3. (a and b) Possible arrangements of V_4O_{10} clusters in the structural model of type IIb. Only V cations are shown. The cubes show the fluorite subcells.

Another modification of the type IIa structure is possible; here the unit cell parameters are doubled and all V_4O_{10} tetrahedra in the (001) unit cell plane have their out-of-plane vanadium cations above the (001) plane. However, the positions of the V_4O_{10} tetrahedra within the rows (see Fig. 3b) are rather different from those shown in Fig. 3a. In this second possibility, the V_4O_{10} tetrahedra in one row have shifted along the $[\bar{1}10]$ unit cell direction. Since there is not enough information from HREM images, it is difficult to differentiate experimentally between the two models. It has been noted that the atomic arrangement in the second model is very similar to that in the type IId model discussed below. The latter has been

confirmed by image simulations on at least two principal directions.

Type IIc Structure

The type IIc structure has a unit cell derived from fluorite lattice by the relations

$$a_{\mathrm{IIc}} = \tfrac{3}{2}a_{\mathrm{f}} + \tfrac{3}{2}c_{\mathrm{f}}$$

$$b_{\mathrm{IIc}} = \tfrac{3}{2}b_{\mathrm{f}} + \tfrac{3}{2}c_{\mathrm{f}}$$

$$c_{\mathrm{IIc}} = -\tfrac{3}{2}a_{\mathrm{f}} - \tfrac{3}{2}b_{\mathrm{f}} + 3c_{\mathrm{f}},$$

with unit cell parameters $a = b \approx 1.17$ nm, $c \approx 2.02$ nm, $\alpha = \beta \approx 74.9°$, and $\gamma \approx 60.0°$ determined from SAED patterns. c_{IIc} could be chosen as $-3a_{\mathrm{f}} - 3b_{\mathrm{f}}$. A principal HREM image and the corresponding SAED pattern viewed down the $[1\bar{1}0]$ direction are shown in Fig. 4. Although the projected orientation of this image corresponds to that of the image in Fig. 6, Ref. (*4*), the intensities of the satellite spots in the SAED patterns and the contrast pattern of

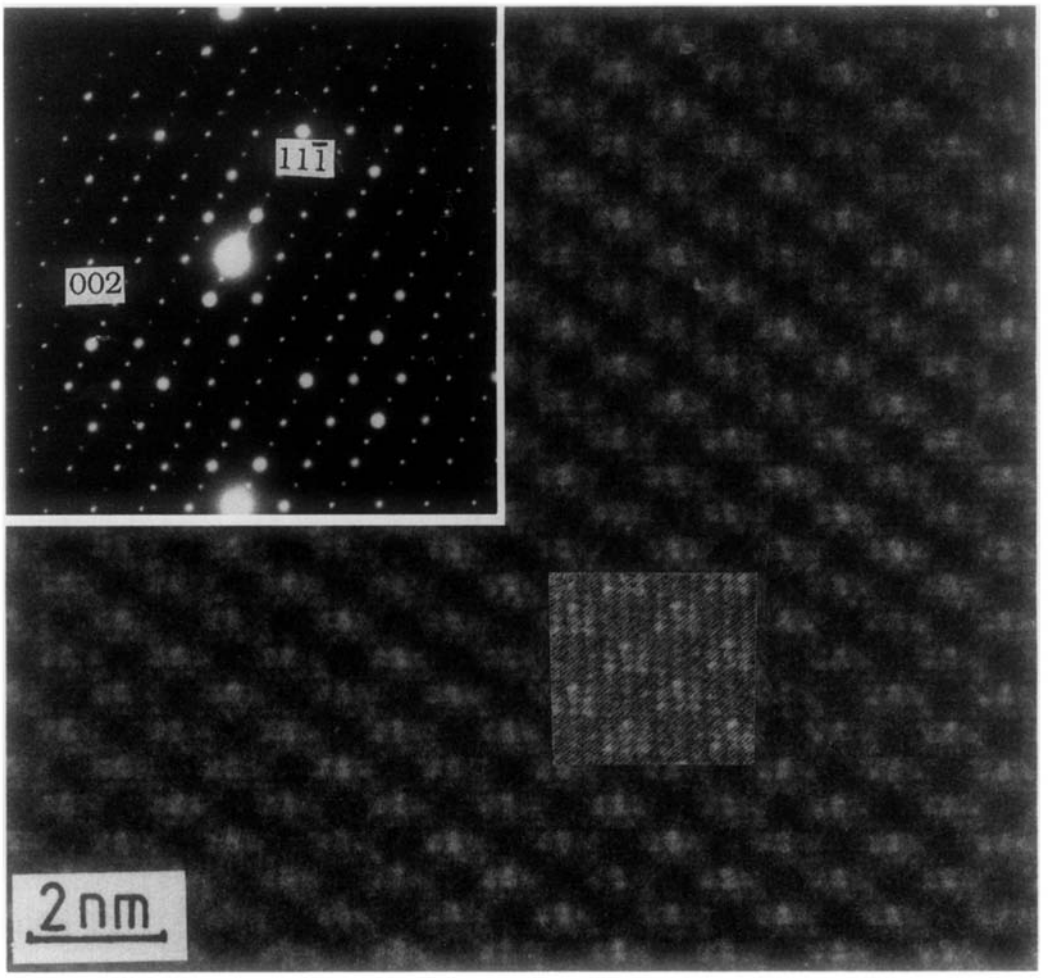

FIG. 4. HREM image and the corresponding SAED pattern of the type IIc structure from $6Bi_2O_3$–V_2O_5, viewed down the $[1\bar{1}0]$ direction of the fluorite sublattice. The inset is a simulated image from the model shown in Fig. 5. The calculation conditions are 8 nm specimen thickness and 150 nm defocus.

the HREM image indicate close to hexagonal symmetry. The structure is also very closely related to type IIa, since $a_{IIc} \approx a_{IIa}$, $b_{IIc} \approx b_{IIa}$ and the arrangement of V_4O_{10} clusters on the main (111) plane is the same as that in type IIa. The difference between c_{IIc} and c_{IIa} is a result of a shift of V_4O_{10} on the main (111) plane. A structural model of type IIc is shown in Fig. 5. The composition of the whole unit cell is $Bi_{46}V_8O_{89}$; i.e., the same as for type IIa. It is likely that the 19 oxygen vacancies are located around the vanadium cations. Image simulation for this model is successful in matching the observed image, as shown in the inset of Fig. 4.

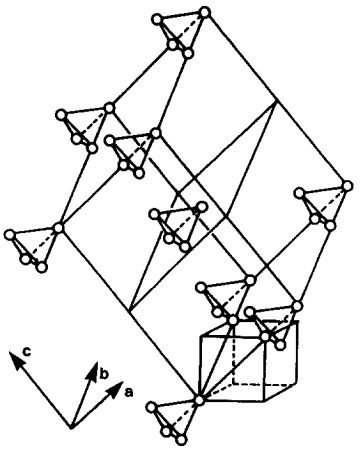

FIG. 5. V_4O_{10} arrangement in the structural model of type IIc. Only V cations are shown. The cube shows the fluorite subcell.

Type IId Structure

The type IId structure is the majority phase in the $6Bi_2O_3$–V_2O_5 sample which was prepared using NaCl as a flux. Several sets of SAED patterns from single microcrystals have been recorded by tilting the specimen grids and these have been indexed onto a new triclinic unit cell, which is derived from the fluorite-like subunit cell by the transformation relations

$$a_{IId} = 3a_f + 3c_f$$

$$b_{IId} = 3b_f + 3c_f$$

$$c_{IId} = -\tfrac{3}{2}a_f - \tfrac{3}{2}b_f + 5c_f.$$

The unit cell parameters are $a = b \approx 2.33$ nm, $c \approx 2.99$ nm, $\alpha = \beta \approx 69.89°$, and $\gamma \approx 60.0°$.

An eightfold repeat in the main [111] direction of the fluorite subcell is the most significant characteristic of this structure. Figure 6a shows the principal HREM image on the $[1\bar{1}0]$ direction. Except for the different c dimension, this image has a similar contrast pattern to that for type IIa (Fig. 6 in Ref. (*4*)). Therefore, the structural model of the type IId can be regarded as a modified type IIa. a_{IId} and b_{IId} are identical to a_{IIb} and b_{IIb}, respectively. Two possible arrangements of V_4O_{10} clusters on the main (111) plane of the type IIb structure have been used in the type IId structural image simulations. The arrangement shown in Fig. 3a has not given good image matching on both the $[1\bar{1}0]$ (Fig. 6a) and [110] (Fig. 6b) directions of the fluorite subunit cell. The final model for the type IId structure, using the V_4O_{10} arrangement of Fig. 3b, is shown in Fig. 7. There are three sheets of the V_4O_{10} cluster-containing planes in each unit cell. Two of them contain four V_4O_{10} units on each sheet and the third contains two V_4O_{10} units. Using this model, simulated images match both the observed ones shown in Fig. 6.

The unit cell composition of the type IId model shown in Fig. 7 is $Bi_{248}V_{40}O_{472}$ with 104 oxygen vacancies.

Type IIe Structure

One SAED pattern (shown in Fig. 8) is very unusual, showing fourfold repeats on the (220) direction of the fluorite sublattice. This cannot be indexed onto any of the discussed members of the type II structural family. A new unit cell has to be considered, designated type IIe. If the underlying structural principle of the other members of

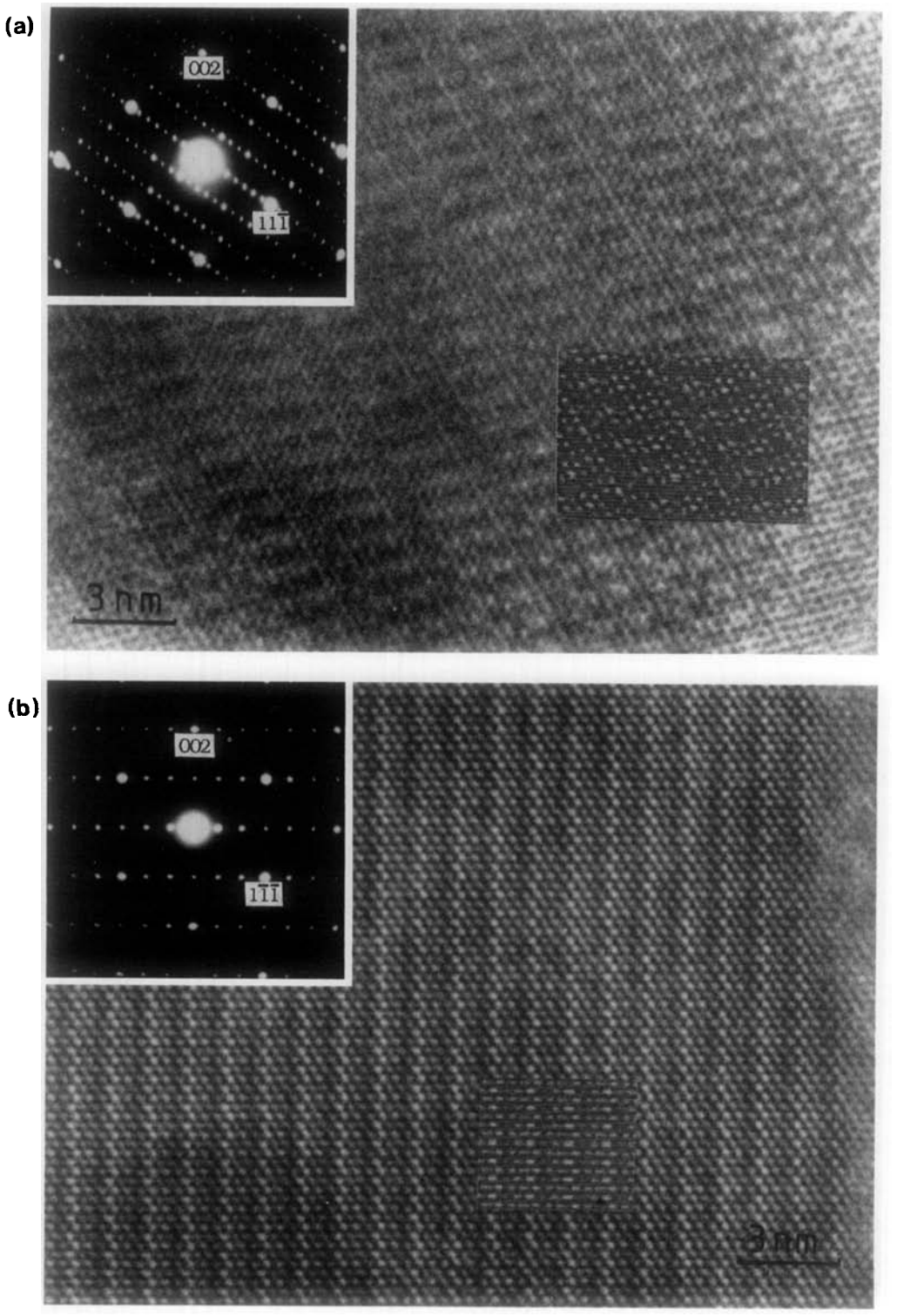

FIG. 6. HREM images and the corresponding SAED patterns of type IId structure taken from $6Bi_2O_3$–V_2O_5, viewed down (a) the [1$\bar{1}$0] and (b) the [110] directions of the fluorite subcell. The insets are simulated images from the model shown in Fig. 7, with the calculation conditions of 8 nm thickness, 140 nm (a), and 120 nm (b) lens defocusses.

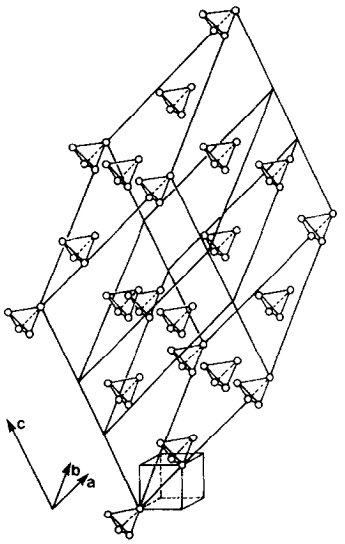

FIG. 7. V_4O_{10} arrangement in the structural model of type IId. Only V cations are shown. The cube shows the fluorite subcell.

the type II family is still applicable for the type IIe, i.e., all V_4O_{10} clusters lie on the main (111) plane of the fluorite sublattice to form a triclinic structure, then the smallest possible unit cell could be derived from the fluorite lattice by the transformation relations

$$a_{\mathrm{IIe}} = 2a_{\mathrm{f}} + 2c_{\mathrm{f}}$$
$$b_{\mathrm{IIe}} = 2b_{\mathrm{f}} + 2c_{\mathrm{f}}$$
$$c_{\mathrm{IIe}} = -\tfrac{1}{2}a_{\mathrm{f}} - \tfrac{1}{2}b_{\mathrm{f}} + 3c_{\mathrm{f}}.$$

The resultant unit cell parameters are $a = b \approx 1.56$ nm, $c \approx 1.70$ nm, $\alpha = \beta \approx 97.7°$, and $\gamma \approx 60.0°$. A possible model is shown in Fig. 9. The unit cell composition of the suggested model is $Bi_{28}V_4O_{52}$. An advantage of this model is that, viewed down the [110] direction of the fluorite lattice, the simulated projection of vanadium cations gives an average image contrast as observed in the experimental image (Fig. 8), instead of strong superlattice fringes shown by the image of Fig. 6b of the type IId structure.

Type IIf Structure

For the composition $4Bi_2O_3$–V_2O_5, a single phase with a very large triclinic structure, designated type IIf, has been revealed by HREM studies. Figures 10a and 10b show two SAED patterns viewed down the $[1\bar{1}0]$ and [112] directions of the fluorite sublattice. A 24-fold repeat of the diffraction spots in the main [111] direction indicates a new commensurate member of the type II family. All SAED patterns obtained can be indexed onto a unit cell with $a = b \approx 1.17$ nm, $c \approx 7.62$ nm, $\alpha = \beta \approx 100.0°$, and $\gamma \approx 60.0°$, derived from the fluorite subunit cell by the transformation relations

$$a_{\mathrm{IIf}} = \tfrac{3}{2}a_{\mathrm{f}} + \tfrac{3}{2}c_{\mathrm{f}}$$
$$b_{\mathrm{IIf}} = \tfrac{3}{2}b_{\mathrm{f}} + \tfrac{3}{2}c_{\mathrm{f}}$$
$$c_{\mathrm{IIf}} = -8a_{\mathrm{f}} - 8b_{\mathrm{f}} + 8c_{\mathrm{f}}.$$

Although the HREM image (Fig. 10c) clearly shows the superlattice in the main [111] direction, proving such a large model by means of image simulation is difficult in practice. The whole unit cell contains 216 cations. Since the sample has been confirmed as a single phase with a composition close to the starting composition, $4Bi_2O_3$–V_2O_5, $11V_4O_{10}$ clusters may be present in the type IIf unit cell. On the other hand, a_{IIf} and b_{IIf} are identical to a_{IIa} and b_{IIa}, there being only one V_4O_{10} cluster on each main (111) plane as shown in Fig. 1. Consequently, among the 24 (111) planes, 11 planes contain V_4O_{10} clusters. The unit cell composition of the proposed model becomes $Bi_{172}V_{44}O_{368}$ with 64 oxygen vacancies.

$7Bi_2O_3$–$2V_2O_5$ is basically of type IIf structure. However, it is incommensurate, as indicated by SAED patterns in Fig. 11. A commensurate monoclinic compound, $Bi_{14}V_4O_{31}$, with $a = 1.9720$, $b = 1.1459$, $c = 8.0160$ nm, and $\beta = 90.5°$, reported by Panchenko *et al.* in 1983 (*8*), has not been observed in the present work. $7Bi_2O_3$–$2V_2O_5$

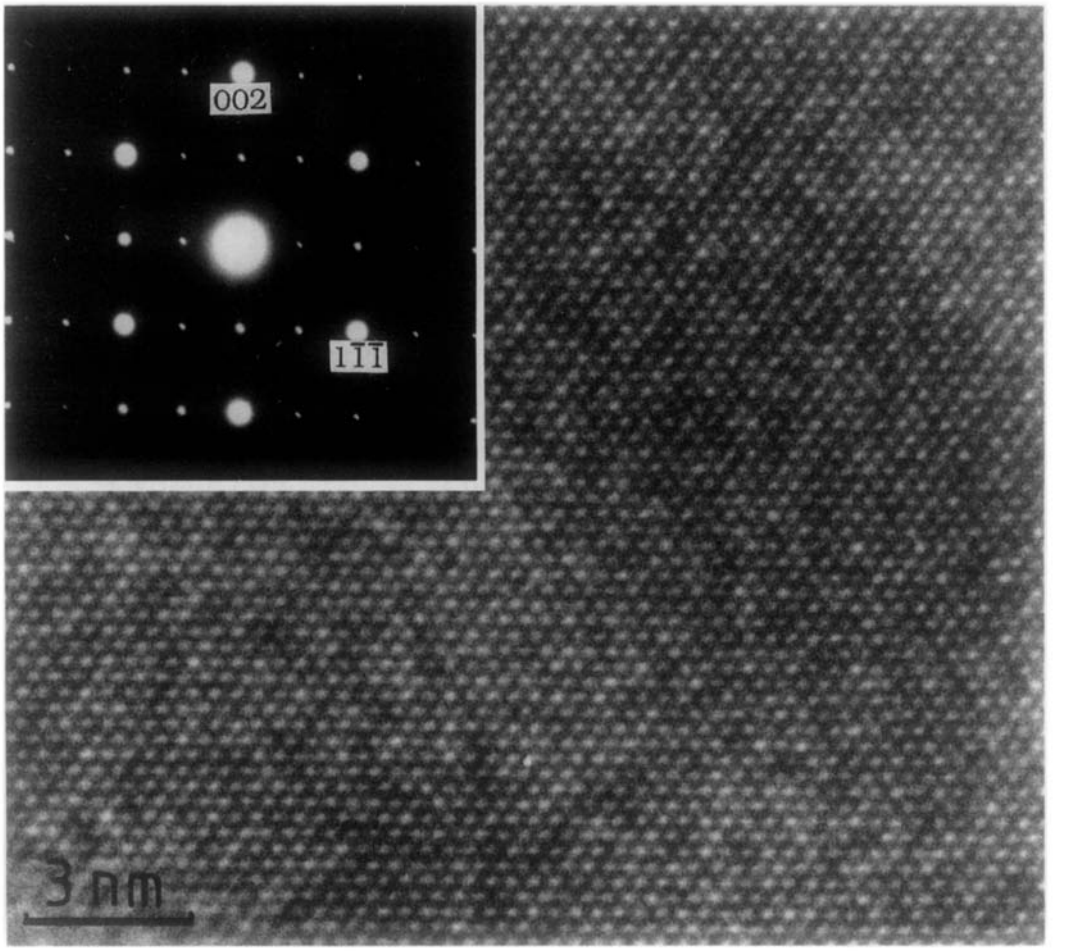

FIG. 8. HREM image and corresponding SAED pattern of the type IIe structure on [110] direction of the fluorite sublattice.

sample is an intermediate phase between type IIf and the orthorhombic phase $Bi_4V_2O_{11}$. The latter has been determined as a γ'-Bi_2MoO_6-like phase (*3*).

Conclusion

In the solid–solution materials with compositions between $6Bi_2O_3$–V_2O_5 and $7Bi_2O_3$–$2V_2O_5$, vanadium cations exist in

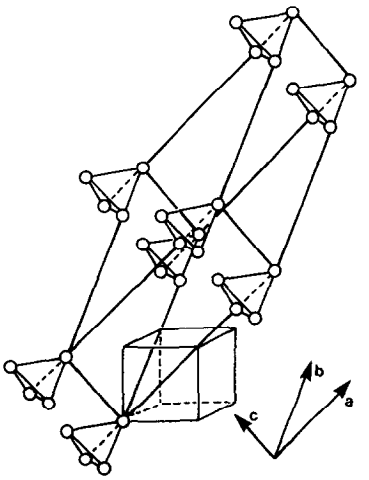

FIG. 9. A possible arrangement of V_4O_{10} in the type IIe structure. Only V cations are shown. The cube shows the fluorite subcell.

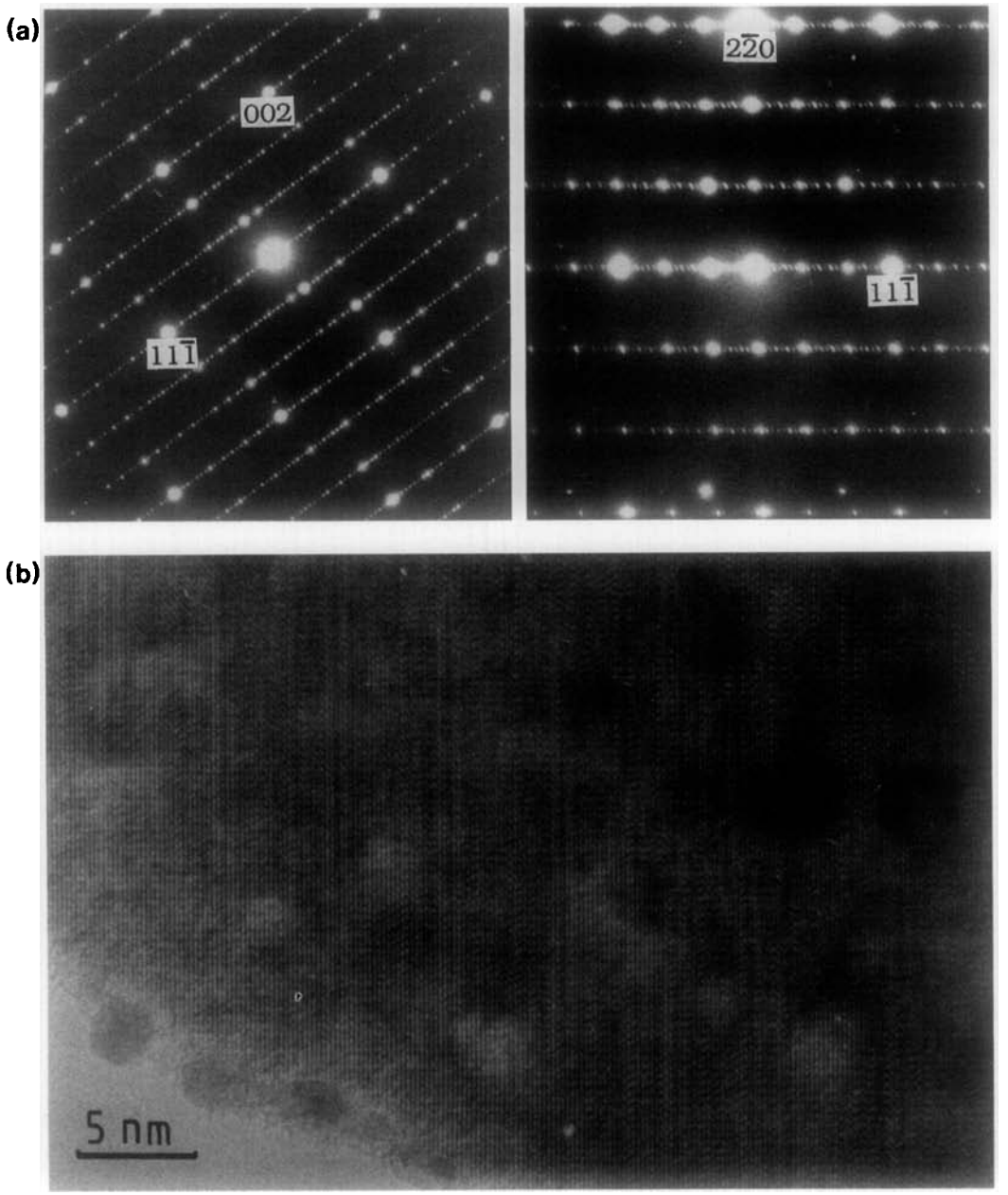

FIG. 10. SAED patterns (a, b) and HREM image (c) of $4Bi_2O_3$–V_2O_5, viewed down the (a) [1$\bar{1}$0] and (b, c) [112] directions of the fluorite subunit cell.

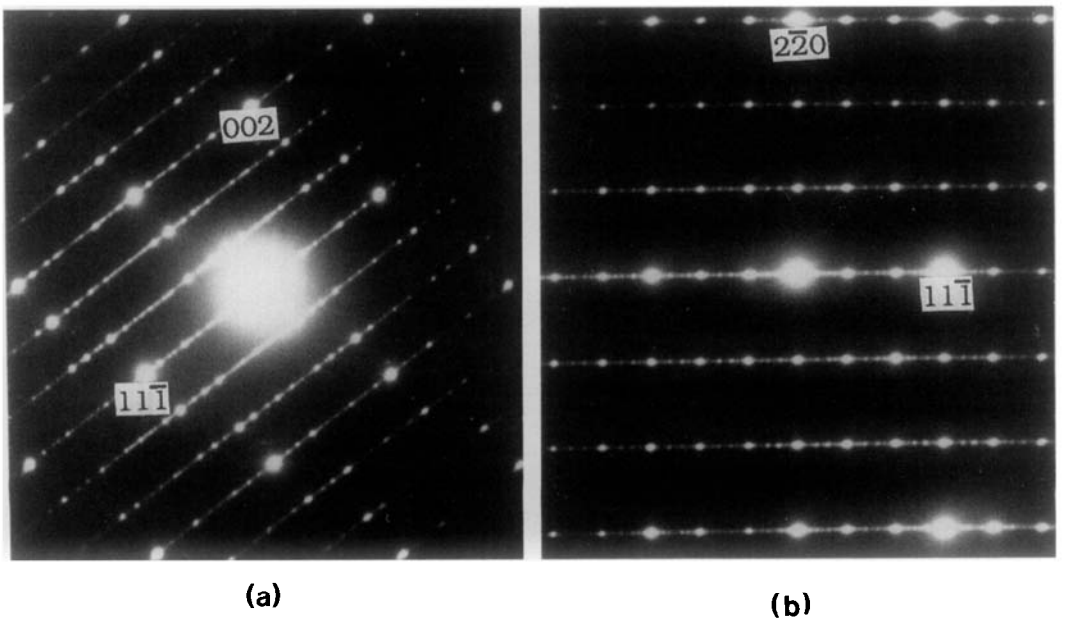

FIG. 11. SAED patterns of $7Bi_2O_3$–$2V_2O_5$, viewed down the (a) [1$\bar{1}$0] and (b) [112] directions of the fluorite subunit cell.

the form of V_4O_{10} clusters inside the defect fluorite δ-Bi_2O_3 host lattice. These V_4O_{10} clusters are ordered on one of the (111) planes of the fluorite lattice, and are separated from one another in such a way as to accommodate as many oxygen vacancies as possible. The arrangement of V_4O_{10} clusters is variable and many triclinic phases have been found and investigated by HREM. These phases have similar underlying structures and properties and have been classified into the type II solid–solution family, following the previous work on the Bi_2O_3–M_2O_5 (M = Nb, Ta, V) systems. In the type II family, the unit cells of all members have been determined by analysis of SAED patterns, the type IIa, type IIc, and type IId structures have been verified by HREM image simulations, and the structures of other members have also been discussed. Studies on the relation between the detailed structures of these materials and their catalytic properties are currently underway.

Acknowledgments

I express my thanks to Dr. D. A. Jefferson for his helpful discussions on this work and Mr. M. Dalton for assistance with preparation of the manuscript.

References

1. W. ZHOU, D. A. JEFFERSON, AND J. M. THOMAS, *Proc. R. Soc. London, Ser. A* **406,** 173 (1986).
2. W. ZHOU, D. A. JEFFERSON, AND J. M. THOMAS, *J. Solid State Chem.* **70,** 129 (1987).
3. W. ZHOU, Ph.D. thesis, University of Cambridge (1987).
4. W. ZHOU, *J. Solid State Chem.* **76,** 290 (1988).
5. H. A. HARWING, *Z. Anorg. Allg. Chem.* **444,** 151 (1978).
6. A. HARRIMAN, J. M. THOMAS, W. ZHOU, AND D. A. JEFFERSON, *J. Solid State Chem.* **72,** 126 (1988).
7. J. M. THOMAS, D. WALLER, AND W. ZHOU, manuscript in preparation.
8. T. V. PANCHENKO, V. F. KATKOV, V. KH. KOSTYUK, N. A. TRUSEEVA, AND A. V. SCHMAL'KO, *Ukr. Fiz. Zh. (Russ. Ed.)* **28**(7), 1091 (1983).